Hindawi
Mathematical Problems in Engineering
Volume 2017, Article ID 8419257, 11 pages
https://doi.org/10.1155/2017/8419257

Research Article

A Novel Protection Scheme against Fault Resistance for AC Microgrid

Xinrui Liu, Zhiyuan Xie, Qiuye Sun, and Zhiliang Wang

School of Information Science and Engineering, Northeastern University, Shenyang 110819, China

Correspondence should be addressed to Xinrui Liu; liuxinrui@ise.neu.edu.cn

Received 18 August 2016; Revised 2 December 2016; Accepted 12 December 2016; Published 2 February 2017

Academic Editor: Aime' Lay-Ekuakille

The faults characteristics of the lines in AC microgrid are weakened due to the fault resistance, which may refuse protection action. To solve the problems caused by different types of the faults through fault resistance (FTFR, the faults where the fault point resistance is greater than zero) in AC microgrid, a novel FTFR protection scheme based on the active power of 0-frame component or d-frame component consumed by fault resistance is proposed in this paper as the backup protection of FTFR. This proposed protection scheme utilizes the active power of 0-frame component or d-frame component consumed by fault resistance to identify internal FTFR and external faults. It performs well in grid-connected mode and islanded mode by adopting self-adaptive threshold and is not affected by the factors such as the fault position and the fault resistance value. The theoretical analysis and various simulations show that this protection scheme can identify and isolate different types of internal FTFR in AC microgrid with high reliability and high sensitivity.

1. Introduction

AC microgrid is defined as a small distribution system with Distributed Generation (DG) sources, like photovoltaics (PVs), wind turbines (WTs), and so forth, energy storage systems (ESS), and local loads [1, 2]. AC microgrid can operate in grid-connected mode and islanded mode, which can provide reliable and sustained power supply to customers [3].

However, the fault currents for grid-connected microgrid and islanded microgrid are significantly different, the bidirectional flow [4, 5], and the faults characteristics are complex because the inverter is connected to DG sources, which represents a big challenge for AC microgrid protection [6–8]. The protection scheme of AC microgrid can be classified into two categories. The first category includes schemes that rely on communication link to share the protection information among the located devices, the microgrid, and the main system and then to realize the online threshold setting and the self-adaptive coordination with protection. Reference [9] proposes a differential protection scheme using communication-assisted digital relays. References [10, 11] use an adaptive protection strategy, and the protection settings were updated by means of microgrid central controller in accordance with microgrid operating modes, to overcome the impact of two operation modes of microgrid on protection. The second category includes schemes that use offline information from the located relay. In [12], a protection scheme that relies on the sum of zero sequence currents is proposed, and it performs well for single-phase to ground faults and phase to phase faults. Another protection scheme is to use "$dq0$" components of the phase voltage at the DGs and then compare with the reference to detect and isolate the fault in microgrid [13].

The above protection schemes perform well for the solid faults (the faults where the fault point resistance is zero) of AC microgrid; however, they are ineffective against the faults through fault resistance (FTFR, the faults where the fault point resistance is greater than zero). And now most studies are focused on the transmission network protection against fault resistance. In [14], an adaptive impedance relay is proposed by using the differential voltage between the prefault voltage and the fault voltage of the faulted phase at the relay location to enhance the capability against fault

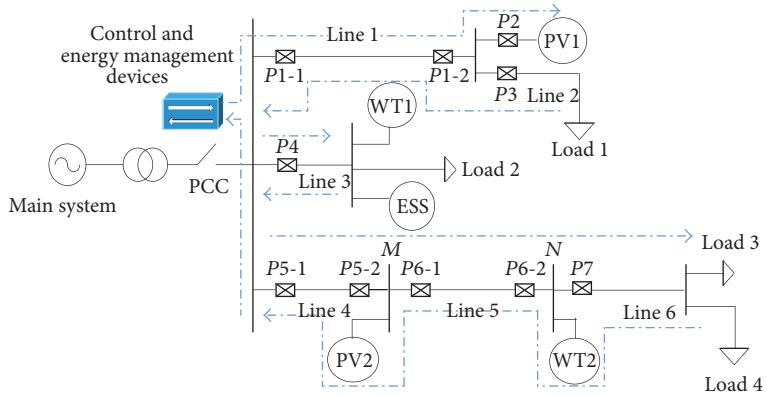

Figure 1: Typical structure of AC microgrid.

resistance, but it is only effective in the initial fault period. Reference [15] introduces the improved differential protection criteria to solve the high-resistance grounding faults under the overload condition, but it is not suitable for all the conditions. Reference [16] proposes a protection scheme based on the active power consumed by the fault resistance, but it only works well for the single-phase high-resistance faults, and it needs phase selecting device. Fault resistance presents a challenge to the protection, and the percentage of various types of FTFR in AC microgrid is significant. Therefore, a novel protection scheme should be proposed to solve this problem.

This paper proposes a novel backup protection scheme against fault resistance for AC microgrid based on the active power of 0-frame component or d-frame component consumed by fault resistance. Different types of FTFR in AC microgrid could be identified by this proposed protection scheme. A self-adaptive threshold is introduced to solve the problem that the sensitivity and reliability of the protection are not satisfactory at the same time due to the factors, for example, the value of fault resistance and fault position. Additionally, the self-adaptive threshold makes this protection perform well in grid-connected mode and islanded mode.

The rest of this paper is summarized as follows. In Section 2, the structure of AC microgrid and the novel protection scheme against fault resistance are analyzed. In Section 3, the self-adaptive threshold setting and the analysis of protection sensitivity are presented. Section 4 focuses on the detail of the protection scheme, including the application scope of this protection scheme. In Section 5, a simulation model is built using PSCAD/EMTDC, and extensive simulations are conducted to verify the effectiveness of this AC microgrid protection in grid-connected mode and islanded mode. Finally, conclusions are presented in Section 6.

2. Structure of AC Microgrid and Analysis of the Novel Protection Scheme against Fault Resistance

2.1. Structure of AC Microgrid. According to the definition of CERTS, Figure 1 shows a typical structure of AC microgrid. AC microgrids consist of DG sources, energy storage systems, local loads, control devices, protection devices, and so forth. It has capabilities of self-control, self-protection, and energy management. Considering the application of protection devices, the reliable power supply, and other factors, the neutral point of AC microgrid system, DG sources, and energy storage systems are not grounded in this paper.

2.2. Analysis of the Novel Protection Scheme against Fault Resistance Based on the 0-Frame Component or d-Frame Component of Active Power Consumed by the Fault Resistance. The faults in power system can be divided into two categories according to the difference of the fault situation. One category is the solid faults, and the other category is FTFR. The characteristic of FTFR is the small fault current; therefore it cannot be detected easily [17]. AC microgrid is a medium-voltage or low-voltage distribution system with the low-voltage level and the small power supply capacity; the faults characteristics of the lines in AC microgrid are weakened due to the fault resistance, which may refuse protection action.

To solve the problems caused by FTFR in AC microgrid, this paper proposes a novel backup protection scheme that can identify and isolate all types of FTFR (single-phase to ground fault, double-phase to ground fault, three-phase to ground fault, and phase to phase fault) effectively. Figure 2 is the equivalent circuit of line MN that occurs in internal FTFR in Figure 1 (due to the low-voltage level of AC microgrid and the fact that the length of the line in AC microgrid is relatively short, the ground capacitance can be ignored), and therefore we take it as an example to analysis the proposed production scheme.

The Park transform (abc-$dq0$) is used to calculate the 0-frame component or d-frame component of the measured currents from M side and N side, as shown in

$$\begin{bmatrix} i_{Md} \\ i_{Mq} \\ i_{M0} \end{bmatrix} = \frac{2}{3} \cdot \begin{bmatrix} \cos\theta & \cos(\theta - 120^\circ) & \cos(\theta + 120^\circ) \\ -\sin\theta & -\sin(\theta - 120^\circ) & -\sin(\theta + 120^\circ) \\ \frac{1}{2} & \frac{1}{2} & \frac{1}{2} \end{bmatrix} \begin{bmatrix} i_{Ma} \\ i_{Mb} \\ i_{Mc} \end{bmatrix}, \quad (1)$$

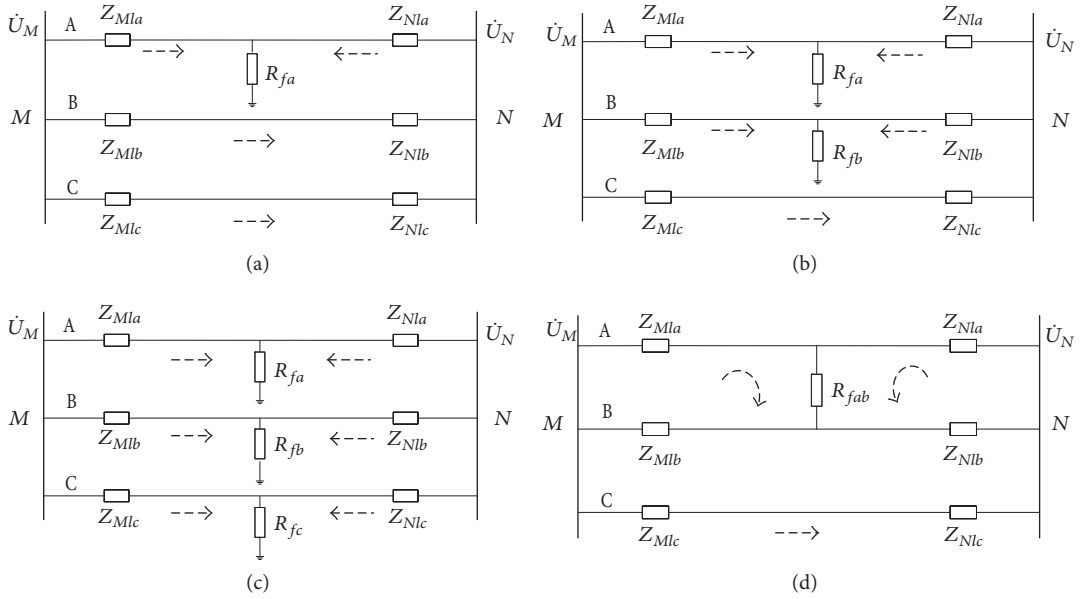

Figure 2: Equivalent circuits for internal FTFR. (a) Single-phase to ground internal FTFR. (b) Double-phase to ground internal FTFR. (c) Three-phase to ground internal FTFR. (d) Phase-phase to ground internal FTFR.

where $\theta = \omega t + \theta_0$, θ_0 is the phase between a-frame and d-frame when $t = 0$, and the 0-frame components of the measured currents at M side and N side are $i_{M0} = (1/3)(i_{Ma} + i_{Mb} + i_{Mc})$ and $i_{N0} = (1/3)(i_{Na} + i_{Nb} + i_{Nc})$; thus when the frequency is definite, we have

$$\begin{aligned} \dot{I}_{M0} &= \frac{1}{3}\left(\dot{I}_{Ma} + \dot{I}_{Mb} + \dot{I}_{Mc}\right), \\ \dot{I}_{N0} &= \frac{1}{3}\left(\dot{I}_{Na} + \dot{I}_{Nb} + \dot{I}_{Nc}\right). \end{aligned} \tag{2}$$

In order to utilize the self-characteristics of fault resistance, the calculation formula of the equivalent fault resistance in various cases is defined as

$$\begin{aligned} \left|Z_f\right| = \big|&Z_{Ma} + Z_{Mb} + Z_{Mc} + Z_{Na} + Z_{Nb} + Z_{Nc} - Z_{la} \\ &- Z_{lb} - Z_{lc}\big| = \left|\frac{\dot{U}_{Ma}}{\dot{I}_{Ma}} + \frac{\dot{U}_{Mb}}{\dot{I}_{Mb}} + \frac{\dot{U}_{Mc}}{\dot{I}_{Mc}} + \frac{\dot{U}_{Na}}{\dot{I}_{Na}} + \frac{\dot{U}_{Nb}}{\dot{I}_{Nb}}\right. \\ &\left. + \frac{\dot{U}_{Nc}}{\dot{I}_{Nc}} - Z_{la} - Z_{lb} - Z_{lc}\right|, \end{aligned} \tag{3}$$

where $|Z_f|$ is the equivalent form of the fault resistance and Z_{Ma}, Z_{Mb}, Z_{Mc}, Z_{Na}, Z_{Nb}, and Z_{Nc} are the measured impedances at M side and N side of A-phase, B-phase, and C-phase, respectively. $\dot{U}_{Ma}$, $\dot{U}_{Mb}$, $\dot{U}_{Mc}$, $\dot{U}_{Na}$, $\dot{U}_{Nb}$, and $\dot{U}_{Nc}$ are the measured voltages at M side and N side of A-phase, B-phase, and C-phase, respectively. $\dot{I}_{Ma}$, $\dot{I}_{Mb}$, $\dot{I}_{Mc}$, $\dot{I}_{Na}$, $\dot{I}_{Nb}$, and $\dot{I}_{Nc}$ are the measured currents at M side and N side of A-phase, B-phase, and C-phase, respectively. $Z_{la} = Z_{Mla} + Z_{Nla}$, $Z_{lb} = Z_{Mlb} + Z_{Nlb}$, and $Z_{lc} = Z_{Mlc} + Z_{Nlc}$ are the definite line impedances of A-phase, B-phase, and C-phase, respectively.

Remark 1. In AC microgrid, firstly the currents or voltages need to be resolved into direct current (DC) term, fundamental sinusoidal term, and multiple sinusoidal terms (harmonic wave) using Fourier transform; then fundamental sinusoidal terms of the measured currents or voltages are extracted, which are used in (3) as the measured currents or voltages. Therefore, the values of $|Z_f|$, P_{R_f0}, and P_{R_fd} (mentioned below) are not affected although the currents or voltages of (3) are not sinusoidal wave for some loads (e.g., uncontrolled rectifier load), so the proposed analysis and protection scheme are still effective.

According to the 0-frame component or d-frame component of the measured currents at M side and N side, the equivalent fault resistance can be calculated. The proposed protection scheme is analyzed in various cases as follows.

2.2.1. Single-Phase to Ground Internal FTFR. As can be seen from Figure 2(a), the measured currents at M side and N side are $\dot{I}_{Ma} = \dot{I}_{Mfa}$, $\dot{I}_{Na} = \dot{I}_{Nfa}$, $\dot{I}_{Mb} = -\dot{I}_{Nb}$, and $\dot{I}_{Mc} = -\dot{I}_{Nc}$ when the internal single-phase to ground FTFR (A-phase to ground, e.g.) takes place. Therefore, the 0-frame components of the measured currents at M side and N side are

$$\begin{aligned} \dot{I}_{M0} &= \frac{1}{3}\left(\dot{I}_{Mfa} + \dot{I}_{Mb} + \dot{I}_{Mc}\right), \\ \dot{I}_{N0} &= \frac{1}{3}\left(\dot{I}_{Nfa} + \dot{I}_{Nb} + \dot{I}_{Nc}\right), \end{aligned} \tag{4}$$

where $|Z_f|$ can be calculated by using (3) as (the derivative process is described in Appendix A)

$$\left|Z_f\right| = \left|\frac{\left(\dot{I}_{Mfa} + \dot{I}_{Nfa}\right)^2}{\dot{I}_{Mfa} \cdot \dot{I}_{Nfa}} \cdot R_{fa}\right|. \tag{5}$$

In the aforementioned formulas, $\dot{I}_{Mfa}$ and $\dot{I}_{Nfa}$ are the internal fault currents of A-phase at M side and N side, respectively, and R_{fa} is the fault resistance of A-phase.

2.2.2. Double-Phase to Ground Internal FTFR. As can be seen from Figure 2(b), the measured currents at M side and N side are $\dot{I}_{Ma} = \dot{I}_{Mfa}$, $\dot{I}_{Na} = \dot{I}_{Nfa}$, $\dot{I}_{Mb} = \dot{I}_{Mfb}$, $\dot{I}_{Nb} = \dot{I}_{Nfb}$, and $\dot{I}_{Mc} = -\dot{I}_{Nc}$ when the internal double-phase to ground FTFR (A-phase to ground, B-phase to ground, e.g.) takes place. Therefore, the 0-frame components of the measured currents at M side and N side are

$$\begin{aligned} \dot{I}_{M0} &= \frac{1}{3}\left(\dot{I}_{Mfa} + \dot{I}_{Mfb} + \dot{I}_{Mc}\right), \\ \dot{I}_{N0} &= \frac{1}{3}\left(\dot{I}_{Nfa} + \dot{I}_{Nfb} + \dot{I}_{Nc}\right), \end{aligned} \tag{6}$$

where $|Z_f|$ can be calculated by using (3) as $|Z_f| = |((\dot{I}_{Mfa} + \dot{I}_{Nfa})^2/(\dot{I}_{Mfa}\cdot\dot{I}_{Nfa}))\cdot R_{fa} + ((\dot{I}_{Mfb}+\dot{I}_{Nfb})^2/(\dot{I}_{Mfb}\cdot\dot{I}_{Nfb}))\cdot R_{fb}|$.

In the aforementioned formulas, $\dot{I}_{Mfa}$, $\dot{I}_{Nfa}$, $\dot{I}_{Mfb}$, and $\dot{I}_{Nfb}$ are the internal fault currents of A-phase and B-phase at M side and N side, respectively; R_{fa}, R_{fb} are the fault resistances of A-phase and B-phase, respectively.

2.2.3. Three-Phase to Ground Internal FTFR. As can be seen from Figure 2(c), the three-phase to ground internal FTFR can be analyzed by the 0-frame component of the measured currents when the fault resistance values or the fault positions of A-phase, B-phase, and C-phase are different. And then $\dot{I}_{Ma} = \dot{I}_{Mfa}$, $\dot{I}_{Na} = \dot{I}_{Nfa}$, $\dot{I}_{Mb} = \dot{I}_{Mfb}$, $\dot{I}_{Nb} = \dot{I}_{Nfb}$, $\dot{I}_{Mc} = \dot{I}_{Mfc}$, and $\dot{I}_{Nc} = \dot{I}_{Nfc}$. Therefore, the 0-frame components of the measured currents at M side and N side are

$$\begin{aligned} \dot{I}_{M0} &= \frac{1}{3}\left(\dot{I}_{Mfa} + \dot{I}_{Mfb} + \dot{I}_{Mfc}\right), \\ \dot{I}_{N0} &= \frac{1}{3}\left(\dot{I}_{Nfa} + \dot{I}_{Nfb} + \dot{I}_{Nfc}\right). \end{aligned} \tag{7}$$

The fault currents are shown as $\dot{I}_{Ma} = I_{Mf}\angle\varphi_1$, $\dot{I}_{Mb} = I_{Mf}\angle\varphi_1 - 120^\circ$, $\dot{I}_{Mc} = I_{Mf}\angle\varphi_1 + 120^\circ$, $\dot{I}_{Na} = I_{Nf}\angle\varphi_2$, $\dot{I}_{Nb} = I_{Nf}\angle\varphi_2 - 120^\circ$, and $\dot{I}_{Nc} = I_{Nf}\angle\varphi_2 + 120^\circ$ when the fault resistance value and the fault position of A-phase, B-phase, and C-phase are same, where I_{Mf} and I_{Nf} are the magnitudes of the fault currents at M side and N side, respectively; φ_1 and φ_2 are the phase of fault currents at M side and N side, respectively. Therefore, the 0-frame components of the measured currents at M side and N side become zero.

In this situation, the d-frame components of the measured currents are considered to identify the above fault, and the fault currents at both sides can be expressed as $i_{Ma} = I_{Mf}\cos(\omega t + \varphi_1)$, $i_{Mb} = I_{Mf}\cos(\omega t + \varphi_1 - 120^\circ)$, $i_{Mc} = I_{Mf}\cos(\omega t + \varphi_1 + 120^\circ)$, $i_{Na} = I_{Nf}\cos(\omega t + \varphi_2)$, $i_{Nb} = I_{Nf}\cos(\omega t+\varphi_2-120^\circ)$, and $i_{Nc} = I_{Nf}\cos(\omega t+\varphi_2+120^\circ)$ when the frequency is definite. Therefore, the d-frame components of the measured currents at M side and N side are given as follows [18]:

$$\begin{aligned} i_{Md} &= I_{Mf}\cos\left(\theta_0 - \varphi_1\right), \\ i_{Nd} &= I_{Nf}\cos\left(\theta_0 - \varphi_2\right), \end{aligned} \tag{8}$$

where $|Z_f|$ can be calculated by using (3) as

$$\begin{aligned} \left|Z_f\right| = \Bigg| &\frac{\left(\dot{I}_{Mfa} + \dot{I}_{Nfa}\right)^2}{\dot{I}_{Mfa}\cdot\dot{I}_{Nfa}}\cdot R_{fa} + \frac{\left(\dot{I}_{Mfb} + \dot{I}_{Nfb}\right)^2}{\dot{I}_{Mfb}\cdot\dot{I}_{Nfb}}\cdot R_{fb} \\ &+ \frac{\left(\dot{I}_{Mfc} + \dot{I}_{Nfc}\right)^2}{\dot{I}_{Mfc}\cdot\dot{I}_{Nfc}}\cdot R_{fc}\Bigg|. \end{aligned} \tag{9}$$

In the aforementioned formulas, $\dot{I}_{Mfa}$, $\dot{I}_{Nfa}$, $\dot{I}_{Mfb}$, $\dot{I}_{Nfb}$, $\dot{I}_{Mfc}$, and $\dot{I}_{Nfc}$ are the internal fault currents of A-phase, B-phase, and C-phase at M side and N side, respectively; R_{fa}, R_{fb}, and R_{fc} are the fault resistances of A-phase, B-phase, and C-phase, respectively.

2.2.4. Phase-Phase to Ground Internal FTFR. As can be seen from Figure 2(d), the measured currents at M side and N side are $\dot{I}_{Ma} = \dot{I}_{Mfab}$, $\dot{I}_{Mb} = -\dot{I}_{Mfab}$, $\dot{I}_{Na} = \dot{I}_{Nfab}$, $\dot{I}_{Nb} = -\dot{I}_{Nfab}$, and $\dot{I}_{Mc} = -\dot{I}_{Nc}$ when the internal phase to phase FTFR (A-phase to B-phase, e.g.) takes place. Therefore, the 0-frame components of the measured currents at M side and N side are

$$\begin{aligned} \dot{I}_{M0} &= \frac{1}{3}\left(\dot{I}_{Mfab} - \dot{I}_{Mfab} + \dot{I}_{Mc}\right) = \frac{1}{3}\dot{I}_{Mc}, \\ \dot{I}_{N0} &= \frac{1}{3}\left(\dot{I}_{Nfab} - \dot{I}_{Nfab} + \dot{I}_{Nc}\right) = \frac{1}{3}\dot{I}_{Nc}, \end{aligned} \tag{10}$$

where $|Z_f|$ can be calculated by using (3) as $|Z_f| = |((\dot{I}_{Mfab} + \dot{I}_{Nfab})^2/(\dot{I}_{Mfab}\cdot\dot{I}_{Nfab}))\cdot R_{fab}|$.

In the aforementioned formulas, $\dot{I}_{Mfab}$, $\dot{I}_{Nfab}$ are the internal fault currents between A-phase and B-phase at M side and N side, respectively; R_{fab} is the fault resistance between A-phase and B-phase.

2.2.5. External Faults and Normal Operation. During external faults and normal operation, $|Z_f|$ can be calculated by using (3) and $|Z_f| = 0$.

According to (2), (3), and (8), the active power of 0-frame component or the d-component consumed by the fault resistance can be expressed as

$$P_{R_f0} = \left|\dot{I}_{M0}\right|\cdot\left|\dot{I}_{N0}\right|\cdot\left|Z_f\right|, \tag{11}$$

$$P_{R_fd} = \left|i_{Md}\right|\cdot\left|i_{Nd}\right|\cdot\left|Z_f\right|, \tag{12}$$

where the 0-frame components of measured currents in (11) are used modulus values and the d-frame components of measured currents in (12) are used absolute values.

As the above analysis, $P_{R_f0} > 0$ or $P_{R_fd} > 0$ in all types of internal FTFR, while $P_{R_f0} = 0$ and $P_{R_fd} = 0$ in external faults and normal operation. Therefore, the internal FTFR can be identified and isolated by the proposed protection scheme.

3. Self-Adaptive Threshold Setting and Protection Sensitivity Analysis

In general, external faults are considered to set the protection threshold. During external faults, P_{R_f0} and P_{R_fd} can be calculated by using (11) and (12) as zero in theory; however, in fact the calculations of P_{R_f0} and P_{R_fd} are greater than zero due to the errors of the current transformers and so forth. Therefore, thresholds $P_{R_f0\text{set}}$ and $P_{R_fd\text{set}}$ are necessary to avoid maloperation during external faults and to ensure the high sensitivity during internal FTFR (the sensitivity coefficients should be $K_{\text{sen}} = P_{R_f0}/P_{R_f0\text{set}} \geq 1.2$ and $K_{\text{sen}} = P_{R_fd}/P_{R_fd\text{set}} \geq 1.2$), and the practical protection criteria can be expressed as

$$P_{R_f0} > P_{R_f0\text{set}}, \tag{13}$$

$$P_{R_fd} > P_{R_fd\text{set}}. \tag{14}$$

In external faults cases, P_{R_f0} and P_{R_fd} are different due to different fault types, fault resistance values, fault positions, and the operation modes of microgrid. All types of external faults cannot be maloperation when setting the maximum value of P_{R_f0} and the maximum value of P_{R_fd} as thresholds, respectively. However, this can reduce the sensitivity of the protection, which may refuse protection action in several cases when the internal FTFR takes place.

Self-adaptive threshold setting is introduced in this paper to solve the problem that the reliability and the high sensitivity of the protection cannot be satisfied at the same time. Typically, the measured error of current transformers is 10% in engineering. Assuming external faults occurred near N side, then (the derivative process is described in Appendix B)

$$\begin{aligned} P_{R_f0} &= \left|\dot{I}_{M0}\right| \cdot \left|\dot{I}_{N0}\right| \cdot \left|Z_f\right| \\ &= 0.11 \left|\dot{I}_{N0}\right|^2 \cdot \left|\frac{\dot{U}_{Na}}{\dot{I}_{Na}} + \frac{\dot{U}_{Nb}}{\dot{I}_{Nb}} + \frac{\dot{U}_{Nc}}{\dot{I}_{Nc}}\right|, \end{aligned} \tag{15}$$

$$\begin{aligned} P_{R_fd} &= \left|i_{Md}\right| \cdot \left|i_{Nd}\right| \cdot \left|Z_f\right| \\ &= 0.11 \left|I_{Nf}\right|^2 \cdot \left|\cos\left(\theta_0 - \varphi_1\right)\right| \cdot \left|\cos\left(\theta_0 - \varphi_2\right)\right| \\ &\quad \cdot \left|\frac{\dot{U}_{Na}}{\dot{I}_{Na}} + \frac{\dot{U}_{Nb}}{\dot{I}_{Nb}} + \frac{\dot{U}_{Nc}}{\dot{I}_{Nc}}\right|, \end{aligned} \tag{16}$$

where $\dot{I}_{N0}$ is the 0-frame component of measured current, I_{Nf} is the magnitude of the d-frame component of measured current, $\dot{I}_{Na/Nb/Nc}$ are the measured currents of A-phase, B-phase, and C-phase, and $\dot{U}_{Na/Nb/Nc}$ are the measured voltages of A-phase, B-phase, and C-phase at N side when external faults occur, respectively. Different types of the external faults occurring at N side are analyzed as follows:

$$\begin{aligned} \dot{I}_{N0} &= \frac{1}{3}\left(\dot{I}_{Nfa} + \dot{I}_{Nb} + \dot{I}_{Nc}\right), \\ \left|\frac{\dot{U}_{Na}}{\dot{I}_{Na}} + \frac{\dot{U}_{Nb}}{\dot{I}_{Nb}} + \frac{\dot{U}_{Nc}}{\dot{I}_{Nc}}\right| &= \left|\frac{\dot{U}_{Nfa}}{\dot{I}_{Nfa}} + \frac{\dot{U}_{Nb}}{\dot{I}_{Nb}} + \frac{\dot{U}_{Nc}}{\dot{I}_{Nc}}\right|, \end{aligned} \tag{17}$$

when single-phase to ground (A-phase to ground, e.g.) external fault at N side takes place:

$$\begin{aligned} \dot{I}_{N0} &= \frac{1}{3}\left(\dot{I}_{Nfa} + \dot{I}_{Nfb} + \dot{I}_{Nc}\right), \\ \left|\frac{\dot{U}_{Na}}{\dot{I}_{Na}} + \frac{\dot{U}_{Nb}}{\dot{I}_{Nb}} + \frac{\dot{U}_{Nc}}{\dot{I}_{Nc}}\right| &= \left|\frac{\dot{U}_{Nfa}}{\dot{I}_{Nfa}} + \frac{\dot{U}_{Nfb}}{\dot{I}_{Nfb}} + \frac{\dot{U}_{Nc}}{\dot{I}_{Nc}}\right|, \end{aligned} \tag{18}$$

when double-phase to ground (A-phase to ground and B-phase to ground, e.g.) external fault at N side takes place:

$$\begin{aligned} \dot{I}_{N0} &= \frac{1}{3}\left(\dot{I}_{Nfa} + \dot{I}_{Nfb} + \dot{I}_{Nfc}\right), \\ \left|\frac{\dot{U}_{Na}}{\dot{I}_{Na}} + \frac{\dot{U}_{Nb}}{\dot{I}_{Nb}} + \frac{\dot{U}_{Nc}}{\dot{I}_{Nc}}\right| &= \left|\frac{\dot{U}_{Nfa}}{\dot{I}_{Nfa}} + \frac{\dot{U}_{Nfb}}{\dot{I}_{Nfb}} + \frac{\dot{U}_{Nfc}}{\dot{I}_{Nfc}}\right| \end{aligned} \tag{19}$$

in (15) and (16); and

$$\begin{aligned} \dot{I}_{N0} &= \frac{1}{3}\dot{I}_{Nc}, \\ \left|\frac{\dot{U}_{Na}}{\dot{I}_{Na}} + \frac{\dot{U}_{Nb}}{\dot{I}_{Nb}} + \frac{\dot{U}_{Nc}}{\dot{I}_{Nc}}\right| &= \left|\frac{\dot{U}_{Nfab}}{\dot{I}_{Nfab}} + \frac{\dot{U}_{Nc}}{\dot{I}_{Nc}}\right|, \end{aligned} \tag{20}$$

when phase to phase (A-phase to B-phase, e.g.) external fault at N side takes place.

In the aforementioned formulas, $\dot{I}_{Nfa}$, $\dot{I}_{Nfb}$, $\dot{I}_{Nfc}$, $\dot{U}_{Nfa}$, $\dot{U}_{Nfb}$, and $\dot{U}_{Nfc}$ are the fault currents and fault voltages of A-phase, B-phase, and C-phase measured at N side when phase to ground external faults take place, respectively; $\dot{I}_{Nfab}$ and $\dot{U}_{Nfab}$ are the fault currents and fault voltages between A-phase and B-phase measured at N side when phase to phase external fault takes place, respectively.

Therefore, self-adaptive thresholds can be expressed as follows with reliability coefficient K_r and other errors' coefficient K_α:

$$P_{R_f0\text{set}} = 0.11 K_r K_\alpha \left|\dot{I}_{N0}\right|^2 \cdot \left|\frac{\dot{U}_{Na}}{\dot{I}_{Na}} + \frac{\dot{U}_{Nb}}{\dot{I}_{Nb}} + \frac{\dot{U}_{Nc}}{\dot{I}_{Nc}}\right|, \tag{21}$$

$$\begin{aligned} P_{R_fd\text{set}} &= 0.11 K_r K_\alpha \left|I_{Nf}\right|^2 \left|\cos\left(\theta_0 - \varphi_1\right)\right| \\ &\quad \cdot \left|\cos\left(\theta_0 - \varphi_2\right)\right| \cdot \left|\frac{\dot{U}_{Na}}{\dot{I}_{Na}} + \frac{\dot{U}_{Nb}}{\dot{I}_{Nb}} + \frac{\dot{U}_{Nc}}{\dot{I}_{Nc}}\right|, \end{aligned} \tag{22}$$

where K_r = 1.2~1.3, K_α = 1.1~1.5 in general, $\dot{I}_{N0}$ is the 0-frame component of the current, I_{Nf} is the magnitude of the d-frame component of the current, and $|\dot{U}_{Na}/\dot{I}_{Na} + \dot{U}_{Nb}/\dot{I}_{Nb} + \dot{U}_{Nc}/\dot{I}_{Nc}|$ is the ratio value of three-phase voltages and three-phase currents measured at N side during internal FTFR cases or external faults cases. And the thresholds can be obtained when the fault occurs at M side by a similar procedure.

Remark 2. The thresholds in the proposed protection are the variables, not the fixed values. Different fault types, fault resistance values, and fault positions are as unknown factors

can affect $\dot{I}_{M0}$, $\dot{I}_{N0}$, i_{Md}, i_{Nd}, $|Z_f|$, and $|\dot{U}_{Na}/\dot{I}_{Na} + \dot{U}_{Nb}/\dot{I}_{Nb} + \dot{U}_{Nc}/\dot{I}_{Nc}|$ in (11), (12), (21), and (22), and then they can affect P_{R_f0}, P_{R_fd}, $P_{R_f0\text{set}}$, and $P_{R_fd\text{set}}$. Furthermore, the change of P_{R_f0} is corresponding to $P_{R_f0\text{set}}$, and also the change of P_{R_fd} is corresponding to $P_{R_fd\text{set}}$. Therefore, the self-adaptive threshold can satisfy the reliability and high sensitivity at the same time.

The values of P_{R_f0} and P_{R_fd} in grid-connected mode are larger than those in islanded mode since the microgrid connects to the main grid and the additional power can be received from it, and this represents a big challenge from the threshold setting of the traditional protection. However, the problem can be solved by the self-adaptive threshold that is proposed in this paper.

The logic diagram of the proposed protection scheme is shown in Figure 3. Firstly, (13) is used to identify the internal FTFR. If the output is 1, then the protection action is done when the criteria are satisfied. Otherwise the output is 0, and then (14) is used to identify the internal FTFR; if the output is 1, then the protection action is done when criteria of (14) are satisfied, otherwise the output is 0 and the protection action is not done.

Remark 3. Formula (3) in the paper is the general form of $|Z_f|$ in the three-phase operation. In the islanded mode, the microgrid may be in the open phase operation (single-phase operation or two-phase operation). However (3) is still suitable; the only difference is that some terms of formula (3) cannot be measured. Then, according to (11) and (12), the active power of 0-frame component and the d-component consumed by the fault resistance (P_{R_f0} and P_{R_fd}) are obtained. Similar analysis process for different fault types is omitted for the open phase operation. It can be summarized that P_{R_f0} is used for single-phase to ground internal FTFR and double-phase to ground internal FTFR in two-phase operation, and P_{R_fd} is used for phase-phase to ground internal FTFR in two-phase operation, and P_{R_f0} is used for single-phase to ground internal FTFR in single-phase operation. In conclusion, $P_{R_f0} > 0$ or $P_{R_fd} > 0$ in all types of internal FTFR, while $P_{R_f0} = 0$ and $P_{R_fd} = 0$ in external faults and normal operation. Therefore, the internal FTFR can be identified and isolated by the proposed protection scheme. Therefore, it can be seen that the logical relationship of protection actions in Figure 3 is also suitable.

Remark 4. The changes of $\theta_0 - \varphi_1$ and $\theta_0 - \varphi_2$ can change the values of i_{Md} and i_{Nd} in (8), respectively, and then change the values of P_{R_fd} in (12) and the values of $P_{R_fd\text{set}}$ in (22), respectively. However, we can get $P_{R_fd}/P_{R_fd\text{set}} = 1/(K_rK_\alpha)$ according to (16) and (22) when external faults take place:

$$\begin{aligned}\frac{P_{R_fd}}{P_{R_fd\text{set}}} &= \frac{\left|I_{Mf}\right| \cdot \left|\cos(\theta_0 - \varphi_1)\right| \cdot \left|I_{Nf}\right| \cdot \left|\cos(\theta_0 - \varphi_2)\right| \cdot \left|Z_f\right|}{0.11K_rK_\alpha \left|I_{Nf}\right|^2 \left|\cos(\theta_0 - \varphi_1)\right| \cdot \left|\cos(\theta_0 - \varphi_2)\right| \cdot \left|\dot{U}_{Na}/\dot{I}_{Na} + \dot{U}_{Nb}/\dot{I}_{Nb} + \dot{U}_{Nc}/\dot{I}_{Nc}\right|} \\ &= \frac{\left|I_{Mf}\right| \cdot \left|Z_f\right|}{0.11K_rK_\alpha \left|I_{Nf}\right| \cdot \left|\dot{U}_{Na}/\dot{I}_{Na} + \dot{U}_{Nb}/\dot{I}_{Nb} + \dot{U}_{Nc}/\dot{I}_{Nc}\right|}.\end{aligned} \tag{23}$$

According to (12) and (22) when the internal FTFR takes place, the above ratio includes neither $\theta_0 - \varphi_1$ nor $\theta_0 - \varphi_2$; therefore, the changes of $\theta_0 - \varphi_1$ and $\theta_0 - \varphi_2$ do not influence the proposed protection scheme.

4. Discussion

4.1. Application Scope of the Proposed Protection Scheme. The existing protection schemes perform well for the solid faults in microgrid, and the performance for FTFR is poor. The protection scheme proposed in this paper is applied after the failure of the existing protection schemes suitable for solid faults, as backup protection to ensure the accurate removal of all fault lines in microgrid.

4.2. Influence of Two Kinds of Operation Modes on the Protection Scheme. Since microgrid can operate in grid-connected mode and islanded mode, it is necessary to protect it in both modes of operation. This paper proposes the self-adaptive threshold setting to solve the problem that values of P_{R_f0} and P_{R_fd} are different between the grid-connected mode and the islanded mode. Therefore, the proposed protection scheme can perform well in both modes of operation.

4.3. Influence of Error. Due to the error of current transformers, the values of P_{R_f0} and P_{R_fd} undergo a little change in fact when internal FTFR takes place. However, the influence of the change can be ignored for the proposed protection scheme.

5. Simulation and Results

The test system is built using PSCAD/EMTDC in this paper. The structure of the microgrid system is shown in Figure 1. Parameters for each component are listed in Table 1. Grid-connected mode and islanded mode are the unique characteristics of the microgrid, and the microgrid protection is required to perform well in both modes. Therefore, simulations are conducted in grid-connected mode and islanded mode to verify the proposed protection scheme, respectively.

5.1. Simulations in Grid-Connected Mode. The voltage and frequency of microgrid are maintained by the main system

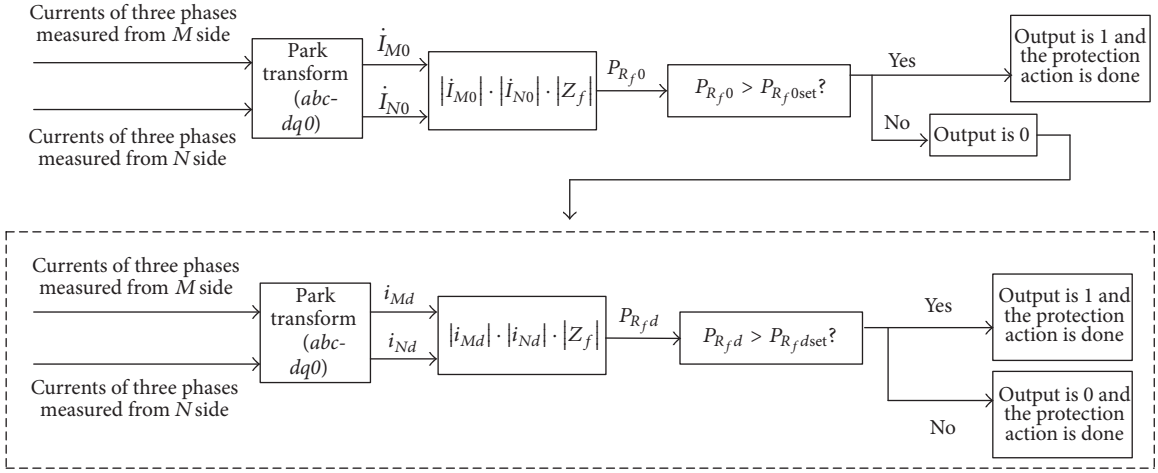

Figure 3: Logic diagram of the proposed protection scheme.

Table 1: System parameters of AC microgrid.

(a)

Component	Data	Parameters		
		R	L	C
Cable ($L1$)	3 km	0.64 Ω/km	0.34 mH/km	0.1 uF/km
Cable ($L2$, $L3$)	1 km	0.64 Ω/km	0.34 mH/km	0.1 uF/km
Cable ($L4$, $L5$, $L6$)	2 km	0.64 Ω/km	0.34 mH/km	0.1 uF/km

(b)

Component	Data
PV 1	1 MVA (λ = 1)
PV 2	1 MVA (λ = 1)
WT1	1 MVA (λ = 0.9)
WT2	0.8 MVA (λ = 0.9)
ESS	2.5 MVA (λ = 1)
Load 1, load 2, load 4	1 MVA (λ = 0.92)
Load 3	0.5 MVA (λ = 0.92)
U_N	10 kV
Main transformer	20 MVA 10 kV/35 kV

when it operates in grid-connected mode. PVs and WTs are taken in MPPT control method, and the output power of each is 0.6 MW, 0.8 MW, 0.75 MW, and 0.5 MW, the odd power is supplied by main system, and ESS is in charging state.

Assuming the faults located in the middle of the MN line, the fault occurs at 0.1 s, and duration of fault is 0.3 s. Single-phase to ground FTFR (A-G), phase to phase FTFR (A-B), and double-phase to ground FTFR (fault resistance value of each phase is the same, A-G and B-G) are taken as the examples to analysis, and the corresponding simulation waveforms are shown in Figures 4(a)–4(c).

Figures 4(a)–4(c) show the values of P_{R_f0} vary with the fault resistance values and the type of faults, and they are all larger than zero. Therefore, internal FTFR can be identified by comparing the values of P_{R_f0}. As shown in Figure 4(b), the value of P_{R_f0} increases with the increase of the fault resistance because P_{R_f0} of phase to phase FTFR is decided by the fault resistance.

For external faults, phase to phase external FTFR (fault resistance is 1 Ω) occurring near N side is taken as an example to analysis, and corresponding simulation waveform is shown in Figure 4(d). The fault occurs at 0.1 s, and the value of P_{R_f0} is almost zero after short time fluctuation. Even considering the influence of the error, the value of P_{R_f0} is greater than zero. However, because its value is very small, the protection action can perform well by using the self-adaptive threshold.

Table 2 shows active power values and the protection threshold setting values of various types of FTFR in different fault positions of line MN when the microgrid operates in grid-connected mode. Fault position = the distance from M side to fault point/the full length of line MN, assuming the fault position of each phase is the same when double-phase fault and three-phase fault take place.

The results in Table 2 show that the values of P_{R_f0}, P_{R_f0set} and P_{R_fd}, P_{R_fdset} of all FTFR types can change with the fault positions, and all are larger than zero in different fault positions. The simulation results are in accordance with the analysis of Section 2.2.

A sensitivity study has been conducted. Figure 5 shows the relationship between P_{R_f0} and P_{R_f0set} when phase to phase internal FTFR takes place. The reliability coefficient K_r is set to 1.3, and the coefficient of the other factors K_α is set to 1.2. In Figure 5, P_{R_f0set} presents a good adaptive performance with the change of the fault positions and the values of fault resistance. And also P_{R_f0set} can change to ensure the high sensitivity of the protection when other types of the internal FTFR take place. Therefore, the protection scheme proposed in this paper can avoid maloperation caused by the external faults and ensure the high sensitivity when the internal FTFR takes place at the same time by using the self-adaptive threshold setting.

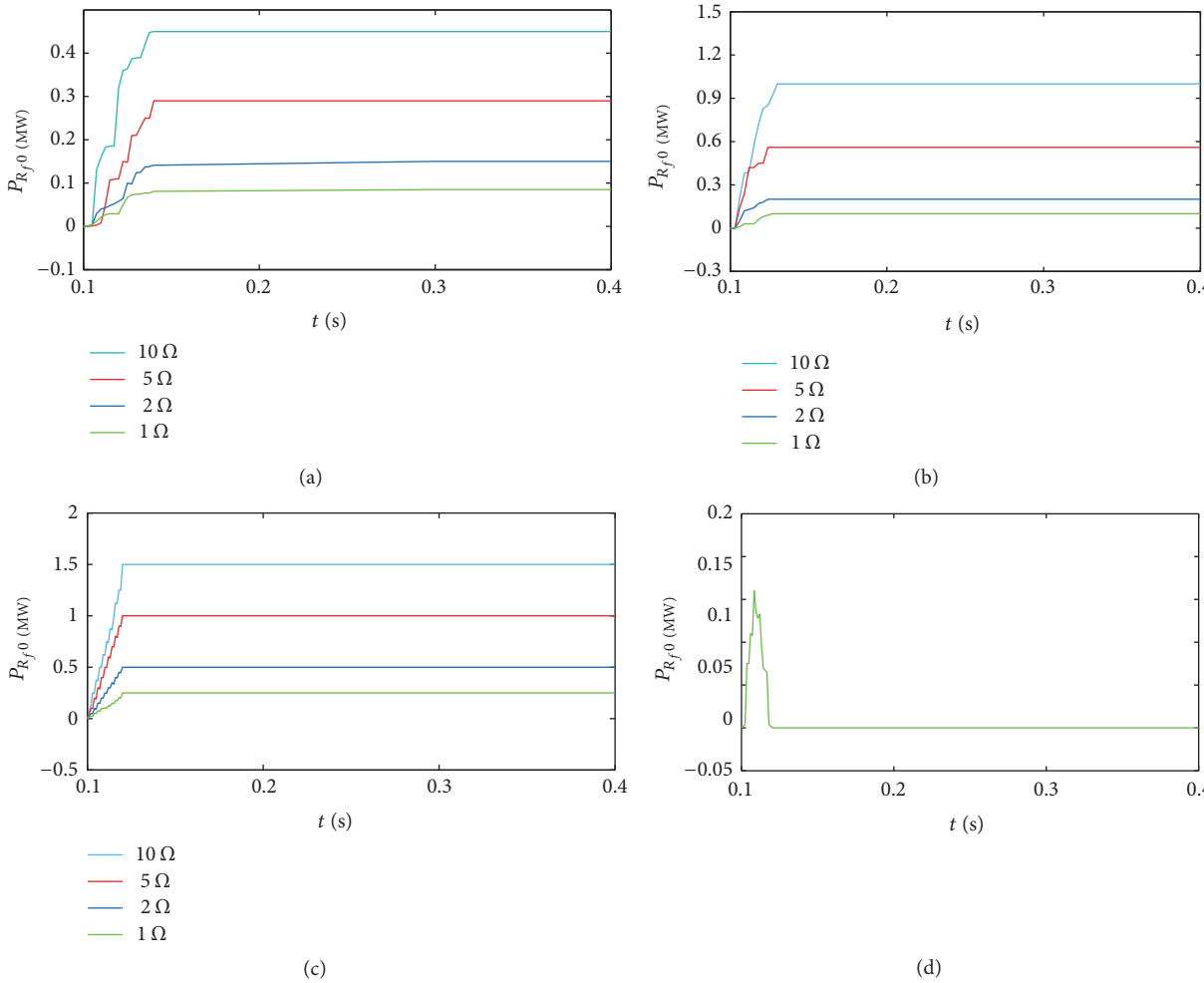

Figure 4: Simulation results of various faults in grid-connected mode. (a) Single-phase internal FTFR. (b) Phase-phase internal FTFR. (c) Double-phase internal FTFR. (d) Phase-phase external FTFR.

Table 2: Active power values and the protection threshold setting values of various types of FTFR in different internal fault positions under grid-connected mode.

Grid-connected mode	Types of fault	Fault position (MW)				
		M side	25%	50%	75%	N side
P_{R_f0} ($P_{R_f0\text{set}}$)	ABG (5 Ω, 5 Ω)	7.52 (0.91)	2.02 (0.80)	0.97 (0.67)	1.83 (0.65)	7.36 (0.60)
	ABG (5 Ω, 6 Ω)	6.80 (1.03)	1.28 (0.59)	0.27 (0.15)	1.14 (0.14)	6.22 (0.12)
	AB (5 Ω)	1.06 (0.22)	0.89 (0.20)	0.51 (0.17)	0.86 (0.14)	1.05 (0.13)
	AG (5 Ω)	4.00 (0.75)	0.78 (0.17)	0.28 (0.12)	0.70 (0.11)	3.86 (0.11)
	ABCG (4 Ω, 5 Ω, 6 Ω)	6.34 (1.08)	1.67 (0.42)	0.23 (0.11)	1.45 (0.11)	5.93 (0.10)
P_{R_fd} ($P_{R_fd\text{set}}$)	ABCG (5 Ω, 5 Ω, 5 Ω)	17.1 (2.84)	6.12 (1.51)	2.05 (1.0)	5.78 (0.09)	16.3 (0.09)

5.2. Simulations in Islanded Mode. The voltage and frequency of microgrid are maintained by ESS when it operates in islanded mode. PVs and WTs are also taken in MPPT control method, and the output power of each is 0.7 MW, 0.9 MW, 0.5 MW, and 0.6 MW, and the odd power is supplied by ESS. Assuming the faults located in the middle of the *MN* line, the fault occurs at 0.1 s, and duration of fault is 0.3 s.

The value of P_{R_f0} is zero when three-phase to ground internal FTFR takes place with the same fault position and the fault resistance value. Therefore, P_{R_fd} is used to identify the fault in this situation, as shown in Figure 6(a). The values of P_{R_fd} with different fault resistances are all larger than zero; therefore, the proposed protection can identify and isolate this fault by using P_{R_fd}.

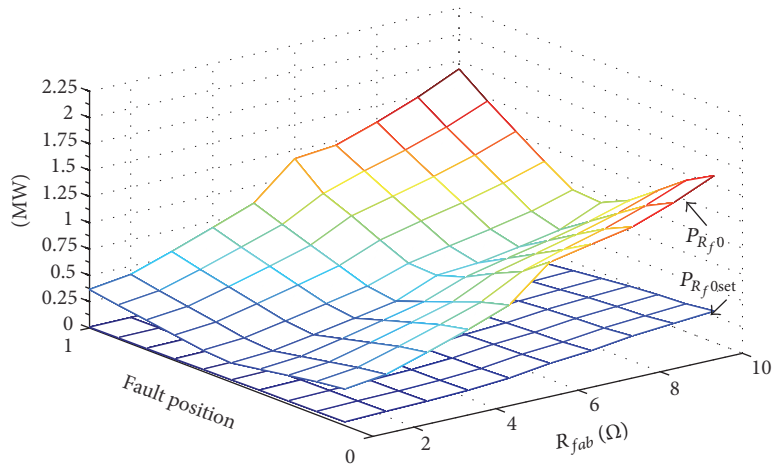

FIGURE 5: Relationship between P_{R_f0} and P_{R_f0set} in phase-phase internal FTFR.

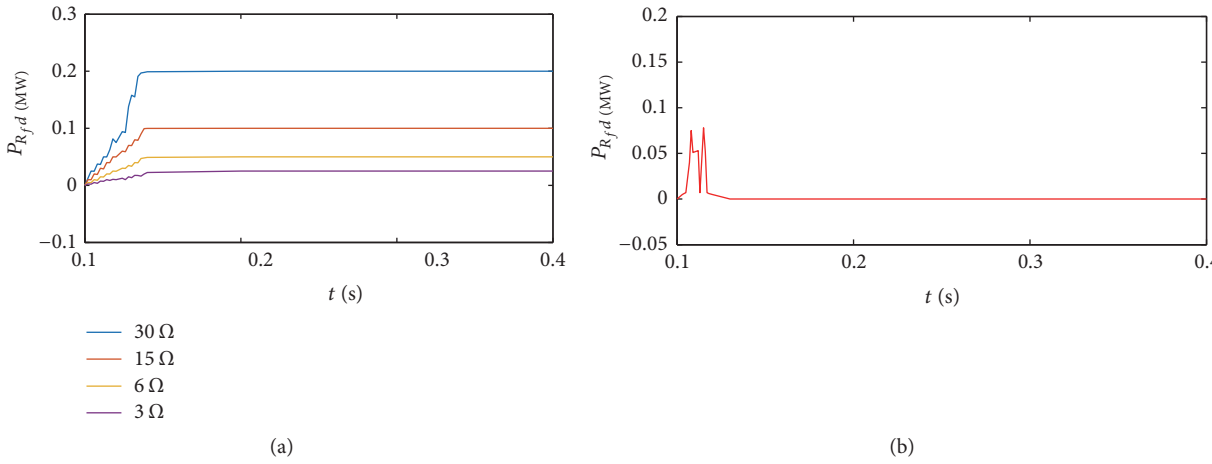

(a) (b)

FIGURE 6: Various faults in islanded mode. (a) Three-phase internal FTFR (fault position and fault resistance value of each phase are the same). (b) Three-phase external solid fault (fault position of each phase is the same).

The values of P_{R_f0} and P_{R_fd} are lower in islanded mode because the overcurrent capability of the electronic devices is usually limited to about 2.0 p.u. However, the sensitivity of the proposed protection can be ensured by the self-adaptive threshold setting.

Figure 6(b) shows P_{R_fd} of the three-phase solid external fault (the fault position of each phase is the same) that takes place near N side. The value of P_{R_fd} is almost zero in steady state, and thus the external fault is recognized. And the proposed protection still performs effectively by taking a suitable threshold, even in the conditions of the errors.

Table 3 shows the active power values and the protection threshold setting values of various types of FTFR in different internal fault positions when AC microgrid operates in islanded mode. As shown, the whole characteristics of P_{R_f0} and P_{R_fd} in islanded mode are the same as those in grid-connected mode; nevertheless, the values of P_{R_f0} and P_{R_fd} are relatively small. The threshold can also change with the operation mode of AC microgrid to ensure isolation of internal FTFR correctly and rapidly.

The above simulation results show that the proposed protection scheme is able to identify internal FTFR correctly in both grid-connected mode and islanded mode, and it also can isolate the internal faults with high reliability and high sensitivity.

6. Conclusions

By using the fault characteristics of the fault resistance in the AC microgrid, this paper proposes a novel protection scheme based on the active power of 0-frame component or d-frame component consumed by fault resistance as the backup protection of FTFR of the lines. It is able to identify and isolate various types of FTFR correctly and rapidly in both operation modes of AC microgrid. Theoretical analysis and simulation results show that the proposed protection scheme has the following characteristics:

Table 3: Active power values and the protection threshold setting values of various types of FTFR in different internal fault positions under islanded mode.

Islanded mode	Types of fault	Fault position (MW)				
		M side	25%	50%	75%	N side
P_{R_f0} ($P_{Rf0\text{set}}$)	ABG (5 Ω, 5 Ω)	1.05 (0.13)	0.26 (0.10)	0.12 (0.08)	0.22 (0.08)	0.97 (0.07)
	ABG (5 Ω, 6 Ω)	0.93 (0.10)	0.17 (0.08)	0.04 (0.02)	0.16 (0.018)	0.89 (0.016)
	AB (5 Ω)	0.30 (0.07)	0.16 (0.04)	0.11 (0.03)	0.14 (0.03)	0.26 (0.02)
	AG (5 Ω)	0.51 (0.10)	0.10 (0.03)	0.04 (0.02)	0.09 (0.019)	0.50 (0.018)
	ABCG (4 Ω, 5 Ω, 6 Ω)	0.91 (0.15)	0.30 (0.08)	0.03 (0.014)	0.26 (0.014)	0.83 (0.013)
P_{R_fd} ($P_{R_fd\text{set}}$)	ABCG (5 Ω, 5 Ω, 5 Ω)	0.97 (0.16)	0.36 (0.09)	0.13 (0.058)	0.32 (0.055)	0.96 (0.05)

(1) It can identify and isolate the internal FTFR validly without using the phase selection device.

(2) It was almost not affected by the operation modes of AC microgrid.

(3) It only needs the measured impedances and the 0-frame component or d-frame component of the measured currents; thus, the data from both sides need not be compared in time. Therefore, the requirement for data synchronization is reduced in this proposed protection scheme.

Appendix

A. The Value of $|Z_f|$ When Different Types of Internal FTFR Occur

This paper defines the current flow from bus to line as the positive direction, assuming the lines current flow from M side to N side is in normal operation:

$$\begin{aligned}
\left|Z_f\right| &= \left|Z_{Ma}+Z_{Mb}+Z_{Mc}+Z_{Na}+Z_{Nb}+Z_{Nc}\right. \\
&\quad \left.-Z_{la}-Z_{lb}-Z_{lc}\right| = \left|\frac{\dot{U}_{Ma}}{\dot{I}_{Ma}}+\frac{\dot{U}_{Mb}}{\dot{I}_{Mb}}+\frac{\dot{U}_{Mc}}{\dot{I}_{Mc}}+\frac{\dot{U}_{Na}}{\dot{I}_{Na}}\right. \\
&\quad \left.+\frac{\dot{U}_{Nb}}{\dot{I}_{Nb}}+\frac{\dot{U}_{Nc}}{\dot{I}_{Nc}}-Z_{la}-Z_{lb}-Z_{lc}\right| \\
&= \left|\frac{\dot{I}_{Mfa}\cdot Z_{Mla}+\left(\dot{I}_{Mfa}+\dot{I}_{Nfa}\right)\cdot R_{fa}}{\dot{I}_{Mfa}}\right. \\
&\quad +\frac{\dot{I}_{Mb}\cdot Z_{lb}+\dot{U}_{Nb}}{\dot{I}_{Mb}}+\frac{\dot{I}_{Mc}\cdot Z_{lc}+\dot{U}_{Nc}}{\dot{I}_{Mc}} \\
&\quad +\frac{\dot{I}_{Nfa}\cdot Z_{Nla}+\left(\dot{I}_{Mfa}+\dot{I}_{Nfa}\right)\cdot R_{fa}}{\dot{I}_{Nfa}}-\frac{\dot{U}_{Nb}}{\dot{I}_{Mb}} \\
&\quad \left.-\frac{\dot{U}_{Nc}}{\dot{I}_{Mc}}-Z_{la}-Z_{lb}-Z_{lc}\right| = \left|\frac{\left(\dot{I}_{Mfa}+\dot{I}_{Nfa}\right)^2}{\dot{I}_{Mfa}\cdot\dot{I}_{Nfa}}\right. \\
&\quad \left.\cdot R_{fa}\right|.
\end{aligned} \tag{A.1}$$

Assuming the lines current flow from N side to M side has the same conclusion, also, the corresponding conclusion can be achieved by the similar procedure when other types of internal FTFR take place.

B. The Values of P_{R_f0} and P_{R_fd} When External Faults Occur

Assuming the current transformers at N side have the error of 10%, thus, $\dot{I}_{Na}=-0.9\dot{I}_{Ma}$, $\dot{I}_{Nb}=-0.9\dot{I}_{Mb}$, $\dot{I}_{Nc}=-0.9\dot{I}_{Mc}$, and, then, $\dot{I}_{N0}=-0.9\dot{I}_{M0}$ and $I_{Nf}=0.9I_{Mf}$. Therefore

$$\begin{aligned}
P_{R_f0} &= \left|\dot{I}_{M0}\right|\cdot\left|\dot{I}_{N0}\right|\cdot\left|Z_f\right| = 1.1\cdot\left|\dot{I}_{N0}\right|^2\cdot\left|\frac{\dot{U}_{Ma}}{\dot{I}_{Ma}}\right. \\
&\quad +\frac{\dot{U}_{Mb}}{\dot{I}_{Mb}}+\frac{\dot{U}_{Mc}}{\dot{I}_{Mc}}+\frac{\dot{U}_{Na}}{\dot{I}_{Na}}+\frac{\dot{U}_{Nb}}{\dot{I}_{Nb}}+\frac{\dot{U}_{Nc}}{\dot{I}_{Nc}}-Z_{la}-Z_{lb} \\
&\quad \left.-Z_{lc}\right| = 1.1\cdot\left|\dot{I}_{N0}\right|^2\left|\frac{\dot{U}_{Ma}}{\dot{I}_{Ma}}+\frac{\dot{U}_{Mb}}{\dot{I}_{Mb}}+\frac{\dot{U}_{Mc}}{\dot{I}_{Mc}}\right. \\
&\quad \left.-\frac{10\dot{U}_{Na}}{9\dot{I}_{Ma}}-\frac{10\dot{U}_{Nb}}{9\dot{I}_{Mb}}-\frac{10\dot{U}_{Nc}}{9\dot{I}_{Mc}}-Z_{la}-Z_{lb}-Z_{lc}\right| \\
&= 1.1\cdot\left|\dot{I}_{N0}\right|^2\cdot\frac{1}{9}\left|\frac{\dot{U}_{Na}}{\dot{I}_{Ma}}+\frac{\dot{U}_{Nb}}{\dot{I}_{Mb}}+\frac{\dot{U}_{Nc}}{\dot{I}_{Mc}}\right| = 1.1 \\
&\quad \cdot\left|\dot{I}_{N0}\right|^2\cdot\frac{1}{10}\left|\frac{\dot{U}_{Na}}{\dot{I}_{Na}}+\frac{\dot{U}_{Nb}}{\dot{I}_{Nb}}+\frac{\dot{U}_{Nc}}{\dot{I}_{Nc}}\right| = 0.11\left|\dot{I}_{N0}\right|^2 \\
&\quad \cdot\left|\frac{\dot{U}_{Na}}{\dot{I}_{Na}}+\frac{\dot{U}_{Nb}}{\dot{I}_{Nb}}+\frac{\dot{U}_{Nc}}{\dot{I}_{Nc}}\right|, \\
P_{R_fd} &= \left|i_{Md}\right|\cdot\left|i_{Nd}\right|\cdot\left|Z_f\right| = 1.1\left|I_{Nf}\right|^2 \\
&\quad \cdot\left|\cos\left(\theta_0-\varphi_1\right)\right|\cdot\left|\cos\left(\theta_0-\varphi_2\right)\right|\cdot\left|\frac{\dot{U}_{Ma}}{\dot{I}_{Ma}}+\frac{\dot{U}_{Mb}}{\dot{I}_{Mb}}\right. \\
&\quad \left.+\frac{\dot{U}_{Mc}}{\dot{I}_{Mc}}+\frac{\dot{U}_{Na}}{\dot{I}_{Na}}+\frac{\dot{U}_{Nb}}{\dot{I}_{Nb}}+\frac{\dot{U}_{Nc}}{\dot{I}_{Nc}}-Z_{la}-Z_{lb}-Z_{lc}\right| \\
&= 1.1\cdot\left|I_{Nf}\right|^2\cdot\left|\cos\left(\theta_0-\varphi_1\right)\right|\cdot\left|\cos\left(\theta_0-\varphi_2\right)\right|
\end{aligned}$$

$$\cdot \left| \frac{\dot{U}_{Ma}}{\dot{I}_{Ma}} + \frac{\dot{U}_{Mb}}{\dot{I}_{Mb}} + \frac{\dot{U}_{Mc}}{\dot{I}_{Mc}} - \frac{10\dot{U}_{Na}}{9\dot{I}_{Ma}} - \frac{10\dot{U}_{Nb}}{9\dot{I}_{Mb}} - \frac{10\dot{U}_{Nc}}{9\dot{I}_{Mc}} - Z_{la} - Z_{lb} - Z_{lc} \right| = 1.1 \cdot \left| I_{Nf} \right|^2 \cdot \left| \cos\left(\theta_0 - \varphi_1\right) \right| \cdot \left| \cos\left(\theta_0 - \varphi_2\right) \right| \cdot \frac{1}{9} \left| \frac{\dot{U}_{Na}}{\dot{I}_{Ma}} + \frac{\dot{U}_{Nb}}{\dot{I}_{Mb}} + \frac{\dot{U}_{Nc}}{\dot{I}_{Mc}} \right| = 1.1 \cdot \left| I_{Nf} \right|^2 \cdot \left| \cos\left(\theta_0 - \varphi_1\right) \right| \cdot \left| \cos\left(\theta_0 - \varphi_2\right) \right| \cdot \frac{1}{10} \left| \frac{\dot{U}_{Na}}{\dot{I}_{Na}} + \frac{\dot{U}_{Nb}}{\dot{I}_{Nb}} + \frac{\dot{U}_{Nc}}{\dot{I}_{Nc}} \right| = 0.11 \left| I_{Nf} \right|^2 \cdot \left| \cos\left(\theta_0 - \varphi_1\right) \right| \cdot \left| \cos\left(\theta_0 - \varphi_2\right) \right| \cdot \left| \frac{\dot{U}_{Na}}{\dot{I}_{Na}} + \frac{\dot{U}_{Nb}}{\dot{I}_{Nb}} + \frac{\dot{U}_{Nc}}{\dot{I}_{Nc}} \right|. \tag{B.1}$$

The corresponding conclusion can be achieved by the similar procedure when external faults take place near M side.

Competing Interests

The authors declare that there is no conflict of interests regarding the publication of this paper.

Acknowledgments

This work is supported by the State Key Program of National Natural Science of China (61433004, 61627809, and 61621004), the Fundamental Research Funds for the Central Universities (N140404003, N130104001), and IAPI Fundamental Research Funds (2013ZCX14).

References

[1] R. H. Lasseter, "MicroGrids," in *Proceedings of the IEEE Power Engineering Society Winter Meeting*, vol. 1, pp. 305–308, New York NY, USA, January 2002.

[2] X. Tang, W. Deng, and Z. Qi, "Investigation of the dynamic stability of microgrid," *IEEE Transactions on Power Systems*, vol. 29, no. 2, pp. 698–706, 2014.

[3] H. Nikkhajoei and R. H. Lasseter, "Distributed generation interface to the CERTS microgrid," *IEEE Transactions on Power Delivery*, vol. 24, no. 3, pp. 1598–1608, 2009.

[4] J. D. F. McDonald, M. Brucoli, and T. C. Green, "Modelling and analysis of fault behaviour of inverter microgrids to aid future fault detection," in *Proceedings of the IEEE International Conference on System of Systems Engineering (SOSE '07)*, pp. 1–6, IEEE, San Antonio, Tex, USA, April 2007.

[5] E. Sortomme, G. J. Mapes, B. A. Foster, and S. S. Venkata, "Fault analysis and protection of a microgrid," in *Proceedings of the 40th North American Power Symposium (NAPS '08)*, pp. 1–6, Alberta, Canada, September 2008.

[6] H. J. Laaksonen, "Protection principles for future microgrids," *IEEE Transactions on Power Electronics*, vol. 25, no. 12, pp. 2910–2918, 2010.

[7] N. Hatziargyriou, H. Asano, R. Iravani, and C. Marnay, "Microgrids," *IEEE Power and Energy Magazine*, vol. 5, no. 4, pp. 78–94, 2007.

[8] B. Kroposki, R. Lasseter, T. Ise, S. Morozumi, S. Papathanassiou, and N. Hatziargyriou, "Making microgrids work," *IEEE Power and Energy Magazine*, vol. 6, no. 3, pp. 40–53, 2008.

[9] E. Casagrande, W. L. Woon, H. H. Zeineldin, and D. Svetinovic, "A differential sequence component protection scheme for microgrids with inverter-based distributed generators," *IEEE Transactions on Smart Grid*, vol. 5, no. 1, pp. 29–37, 2014.

[10] P. Mahat, Z. Chen, B. Bak-Jensen, and C. L. Bak, "A simple adaptive overcurrent protection of distribution systems with distributed generation," *IEEE Transactions on Smart Grid*, vol. 2, no. 3, pp. 428–437, 2011.

[11] H. Laaksonen, D. Ishchenko, and A. Oudalov, "Adaptive protection and microgrid control design for Hailuoto Island," *IEEE Transactions on Smart Grid*, vol. 5, no. 3, pp. 1486–1493, 2014.

[12] H. Nikkhajoei and R. H. Lasseter, "Microgrid protection," in *Proceedings of the IEEE Power Engineering Society General Meeting (PES '07)*, pp. 1–6, Tampa, Fla, USA, June 2007.

[13] M. A. Redfern and H. Al-Nasseri, "Protection of micro-grids dominated by distributed generation using solid state converters," in *Proceedings of the 9th International Conference on Developments in Power Systems Protection (DPSP '08)*, Glasgow, UK, March 2008.

[14] Y. Li, D. Chen, X. Yin, and Z. Zhang, "Research of one new adaptive Mho relay," in *Proceedings of the IEEE Power System Technology*, pp. 2604–2607, Kunming, China, October 2002.

[15] J. Tang and X.-R. Wang, "Current differential protection criterion using steady currents for heavy-load line with high fault resistance," *Proceedings of the Chinese Society of Electrical Engineering*, vol. 28, no. 4, pp. 72–77, 2008.

[16] X. G. Jiang, Z. P. Wang, Z. C. Zhang, and J. Ma, "Single-phase high-resistance fault protection based on active power of transition resistance," *Proceedings of the Chinese Society of Electrical Engineering*, vol. 33, no. 13, pp. 187–193, 2013.

[17] J. L. He, Y. L. Li, X. Z. Dong, and B. Li, *Principle of Electrical System's Relay Protection*, China Electric Power Press, Beijing, China, 4th edition, 2010.

[18] G. Q. Li, *Transient Analysis of Power System*, China Electric Power Press, Beijing, China, 3rd edition, 2007.